IMA Journal of Applied Mathematics (2018) **00**, 1–20
doi:10.1093/imamat/hxy013

The role of tumbling frequency and persistence in optimal run-and-tumble chemotaxis

Julius B. Kirkegaard and Raymond E. Goldstein*
Department of Applied Mathematics and Theoretical Physics, Centre for Mathematical Sciences, University of Cambridge, Wilberforce Road, Cambridge CB3 0WA, UK
*Corresponding author: R.E.Goldstein@damtp.cam.ac.uk

[Received on 13 September 2017; revised on 22 March 2018; accepted on 23 March 2018]

One of simplest examples of navigation found in nature is run-and-tumble chemotaxis. Tumbles reorient cells randomly, and cells can drift towards attractants or away from repellents by biasing the frequency of these events. The post-tumble swimming directions are typically correlated with those prior, as measured by the variance of the reorientation angle distribution. This variance can range from large, in the case of bacteria, to so small that tumble events are imperceptible as observed in choanoflagellates. This raises the question of optimality: why is such a range of persistence observed in nature? Here we study persistent run-and-tumble dynamics, focusing first on the optimization of the linearized chemotactic response within the 2D parameter space of tumble frequency and angular persistence. Although an optimal persistence does exist for a given tumble frequency, in the full parameter space there is a continuum of optimal solutions. Introducing finite tumble times that depend on the persistence can change this picture, illuminating one possible method for selecting tumble persistence based on species-specific reorientation dynamics. Moving beyond linear theory we find that optimal chemotactic strengths exist, and that these maximize reaction when swimming in a wrong direction but have little or no reaction when swimming with even the slightest projection along the chemoattractant gradient.

Keywords: chemotaxis; run-and-tumble; microorganisms.

1. Introduction

Chemotaxis, the ability to navigate concentration fields of chemicals, is a ubiquitous feature of the microscopic world. Performed by uni- and multicellular organisms alike, it represents one of the simplest forms of navigation. Within this simplicity, various strategies exist. For instance, certain spermatozoa measure chemoattractant gradients by swimming in helical trajectories and bias the helical axis to move directly towards the chemoattractant (Friedrich & Juicher, 2007; Jikeli *et al.*, 2015). Green algae can swim towards light-intense regions by measuring light source directions as they rotate around their own swimming axis (Yoshimura & Kamiya, 2001; Drescher *et al.*, 2010) and also bias their navigation by switching between synchronous and anti-synchronous beating of their flagella (Polin *et al.*, 2009). The slime mould *D. discoideum* is large enough to measure directly the spatial concentration gradients in cyclic AMP, along which it navigates (Bonner & Savage, 1947). The epitome of chemotaxis is perhaps the run and tumble of certain peritrichously flagellated bacteria such as *E. coli* (Berg & Brown, 1972).

Run-and-tumble motion is comprised of approximately straight lines (runs) interrupted by reorientation events (tumbles), as shown in Fig. 1. For example, in peritrichous bacteria, the helical flagella rotate counterclockwise and form a coherent bundle during swimming. A tumble is induced when (some of) the flagella reverse their rotational direction and the bundle is disrupted (Fig. 1(a)).

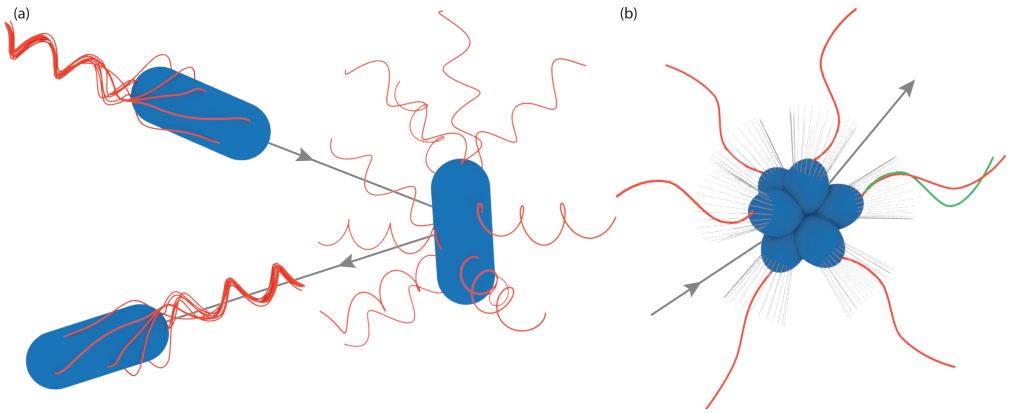

FIG. 1. Run and tumble. (a) Swimming and tumbling of a peritrichous bacterium. During swimming the flagella rotate counterclockwise and form a bundle resulting in a run. Clockwise rotation of one or more flagella breaks the bundle and results in a tumble that reorients the cell. (b) Choanoflagellate colony reorientation event. Each cell's flagellum beats independently of the others. A change in the beating dynamics of one cell (green flagellum) can cause a small reorientation of the colony as a whole.

This creates a large, transient reorientation. Navigation along a gradient of chemoattractant becomes possible if the frequency of tumbling is biased in response to the chemoattractant distribution. This is a type of 'stochastic' navigation in the sense that the organisms that perform it do not swim directly in the desired direction but rather in a random direction and later decide whether such a turn was correct.

The tumbling frequency is modulated through measurements of the variation in concentration of chemoattractants, illustrated by the background of Fig. 2. In an idealized scenario, the reorienting tumbles result in unbiased new directions, uniformly chosen from the unit sphere, but this is not typically the case. Instead, a persistence with the previous direction is present (Berg & Brown, 1972). In fact, for some species, the individual reorientations are so small that they are hardly observable. This is the case in colonies of choanoflagellates (Kirkegaard *et al.*, 2016a), within which the flagella beat independently (Kirkegaard *et al.*, 2016b) and a reorientation event may simply arise from slight modulation of the beating of a single flagellum (Fig. 1(b)). These smaller tumbles, or directionally persistent tumbles, add up to a smoother swimming while still allowing navigation. Figure 2 shows two realizations of run-and-tumble swimming. In blue is the case of full-reorientation tumbles and in red is very persistent tumbles occurring with higher frequency. Over long timescales both of these swimmers perform random walks biased in the direction of the chemoattractant signal.

A strong theoretical understanding of chemotaxis exists (Tindall *et al.*, 2008a,b), including the filtering of chemoattractant signals to which the cells react (Segall *et al.*, 1986; Celani & Vergassola, 2010), the fundamental limits of measurement accuracy of such signals (Mora & Wingreen, 2010) and the limits they impose on navigation (Hein *et al.*, 2016). Theories of chemotaxis are typically developed in the weak-chemotaxis limit (Celani & Vergassola, 2010; Locsei, 2007; Locsei & Pedley, 2009; Reneaux & Gopalakrishnan, 2010; Mortimer *et al.*, 2011), the linear theory of which provides accurate explanations of many experimental observations. Theory (Locsei, 2007) and simulation (Nicolau *et al.*, 2009) of chemotactic bacteria have also showed that for otherwise equal chemotactic parameters directional persistence of tumbles, as observed in experiments, can lead to enhanced chemotaxis.

This raises a more general question: could the effect of changing one parameter, such as directional persistence, be compensated by simultaneously changing another? Here, we address this question

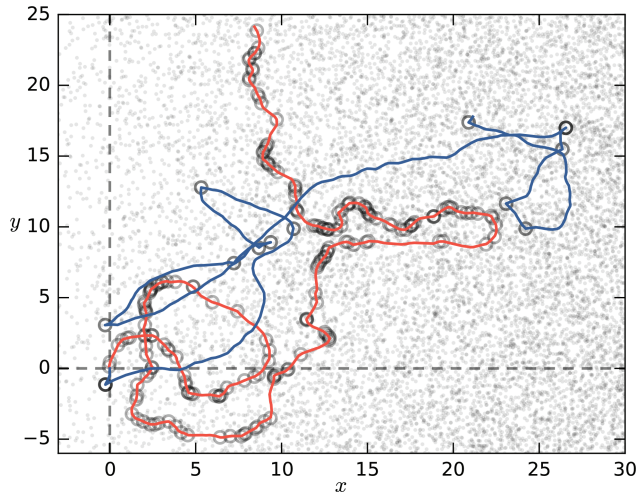

FIG. 2. Run-and-tumble trajectories. Both simulated trajectories drift to the right, starting from the origin. Full tumbles are shown in blue $(k = 0, \lambda_0 = 0.1\,\mathrm{s}^{-1})$ and persistent but frequent tumbles, in red $(k = 10, \lambda_0 = 2.0\,\mathrm{s}^{-1})$. Circles indicate tumbles. Shared parameters: $D_r = 0.1\,\mathrm{s}^{-1}$, $\beta = 1/2$, $\gamma = 1\,\mathrm{s}^{-1}$.

of global optimality and examine effects that lead to the existence of optima. For example, in linearized theories, the drift velocities for large chemotactic strength and for steep gradients can become unbounded, and thus the evaluation of one effect is done at fixed chemotactic response. But microorganisms do not have the restrictions that come with choosing theories that are analytically tractable. In real systems, the drift velocity will be limited (trivially) due to the finite swimming speed of the organisms and (more importantly) by uncertainties of measurements in noisy environments combined with diffusion. Throughout this study we optimize for the performance of a single organism, neglecting population effects (Peaudecerf & Goldstein, 2015).

2. Model

The model of chemotaxis used here assumes that organisms determine concentration gradients by comparing their concentration measurements at different times as they move through the medium, rather than detecting gradients over their own body, as is possible for organisms considerably larger than bacteria (Berg & Purcell, 1977). To be precise, we assume that as a cell swims it measures only the local chemoattractant concentration $c(\boldsymbol{x}, t)$ at its present position $\boldsymbol{x}$. Moreover, in this section the concentration is taken to be linear in position, $c(\boldsymbol{x}) = c_0 + \alpha\, x$, allowing the notation $c(t) = c(\boldsymbol{x}(t))$ for a given trajectory $\boldsymbol{x}(t)$. Cells are thought to store the history of these measurements and use this to bias their tumbling frequency λ. In the present model, this is embodied by the relationship $\lambda = \lambda_0 \lfloor 1 + q \rfloor$, where $\lfloor \cdot \rfloor = \max(0, \cdot)$. Here, q is the biaser, determined by a linear convolution of c,

$$q(t) = \int_0^\infty c(t - t')\, \kappa(t')\, \mathrm{d}t'. \tag{2.1}$$

We take the kernel to be one studied previously and which corresponds well to experimental measurements (Segall *et al.*, 1986; Celani & Vergassola, 2010),

$$\kappa(t) = \frac{\beta\gamma^2}{\alpha\, v} e^{-\gamma t}\left[\frac{(\gamma t)^2}{2} - \gamma\, t\right], \tag{2.2}$$

where v is the swimming speed and γ is the memory timescale of past measurements. The normalization is chosen such that $\max|q| = \beta$ in the absence of noise, and hence β solely specifies the chemotactic strength. The kernel satisfies $\int \kappa(t)\,\mathrm{d}t = 0$ which gives perfect adaptation to any background chemoattractant concentration. This criterion arises naturally from maximizing the minimum chemotactic efficiency over all chemoattractant profiles (Celani & Vergassola, 2010). In particular, this is an important feature that will not arise from maximizing drift velocity alone and which we thus impose *a priori* here.

We consider cells swimming in two dimensions in an instantaneous direction $\theta(t)$ with velocity v and discuss the 3D case in Appendix D. This direction is modulated by both rotational diffusion as $\mathrm{d}\theta = \sqrt{2D_r}\,\mathrm{d}W$, where W is a standard Wiener process, and by tumbles, the size of which is chosen from a von Mises distribution with parameter k, $p(\Delta\theta) = \exp(k\cos(\Delta\theta))/2\pi I_0(k)$, where I_n are the modified Bessel functions of the first kind. Thus, k specifies the persistence of the tumbles, $k = 0$ corresponding to full tumbles.

3. Measurement timescale

If the time $1/\lambda_0$ between tumbles is too long compared to the rotational diffusion time $1/D_r$, the trajectories will be reoriented by rotational diffusion and the organism will have lost the ability to bias its motion in any useful way. Thus, the biasing of tumbles must outcompete rotational diffusion and we expect $\lambda_0 \gtrsim D_r$. In the absence of measurement noise, and if the organism can make instantaneous measurements ($\gamma \to \infty$), increasing the chemotactic strength will monotonically increase the chemotactic drift, and in the limit $\beta \to \infty$ chemotaxis becomes perfect despite the hindering effects of rotational diffusion. But we emphasize that this is only possible in the absence of measurement noise. Here, in contrast, we are interested in the noise-limited situation, and with noise comes another timescale, that over which accurate measurements can be made (see Appendix F for a simple lattice calculation illustrating this point).

To illuminate this situation we perform simulations in which cells are placed in a constant gradient (linear increase) of discrete chemoattractants. In a periodic $2L \times 2L$ box, N molecules are placed, decreasing linearly in concentration from $x = 0$. This is achieved by choosing each molecule's position as $x = L\sqrt{|U_1|}\,\mathrm{sign}(U_1)$, $y = LU_2$, where U_i is uniformly distributed on $[-1, 1]$. Here, $c(t)$ is then defined to be the number of molecules within a cell's area. This can be evaluated efficiently by storing the molecules in a k-D tree (a data structure for fast neighbour lookups), allowing for simulations with billions of molecules.

For the purposes of the present discussion, we define the chemotactic efficiency proportional to the average value of the concentration experienced by the organism in steady state

$$\eta \propto \langle c\rangle = \int c(\boldsymbol{x})P(\boldsymbol{x})\,\mathrm{d}\boldsymbol{x}, \tag{3.1}$$

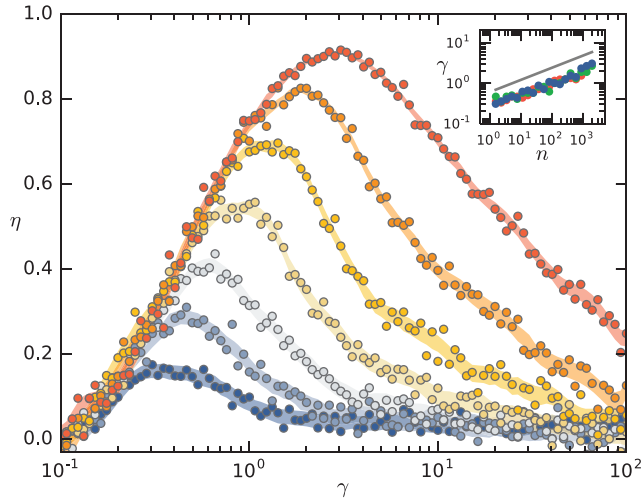

FIG. 3. Chemotactic efficiency as a function of γ. Each curve corresponds to different concentration levels; at the lowest concentration (blue data) each cell senses on average $n \sim 1.5$ molecules, while at the highest (red), $n \sim 2000$ are sensed. Shaded background indicates standard error of the simulations. Inset shows optimal γ as a function of n for $\lambda_0 \in \{0.1, 1.0, 5.0\}\,\mathrm{s}^{-1}$. $D_r = 0.1\,\mathrm{s}^{-1}$, $\gamma = 1\,\mathrm{s}^{-1}$.

where $P(\boldsymbol{x})$ is the steady-state probability distribution. The normalization is chosen such that $\eta = 1$ corresponds to perfect chemotaxis.

Figure 3 shows η as function of the measurement rate γ for various molecular concentrations. The curves clearly reveal the existence of an optimal γ for each choice of the (average) number of molecules sensed. Choosing γ too low means slow reaction, but with γ too high the organism does not have time to make an accurate measurement before previous information is forgotten. Varying the chemoattractant concentration (but not the gradient) shifts the optimal γ. At higher concentrations, the measurement noise is lower (Mora & Wingreen, 2010), and thus less time is needed to make an accurate measurement. The inset of Fig. 3 shows how the optimal γ varies with the concentration, and further shows that, within the resolution of our simulations, this optimum is independent of the base tumbling frequency λ_0. This independence means that we can fix γ to its optimal value without specifying the value of λ_0.

In this noise-dominated regime, γ is thus set by the chemoattractant concentration. If cells are kept in a chemostat with fixed concentration and gradient, as is the case considered here, the optimal γ is thus indicative of the underlying noise levels. In the following sections we fix γ, thus implicitly defining the noise levels. The goal then becomes to find the optimal choice of the remaining parameters for a given γ. Our approach ignores spatial variations in noise, but conclusions made are confirmed by checking them against the full simulation set-up used in this section.

4. Tumbling frequency and persistence

In earlier theoretical work, persistence of tumbles has been shown to enhance the chemotactic drift velocity (Locsei, 2007; Nicolau *et al.*, 2009). Possible rationalizations for this effect include the idea of information relevance; for persistent tumbles, the gradient information (stored in q, (2.1)) remains more relevant than for full tumbles, where a completely random direction is chosen. It has also been

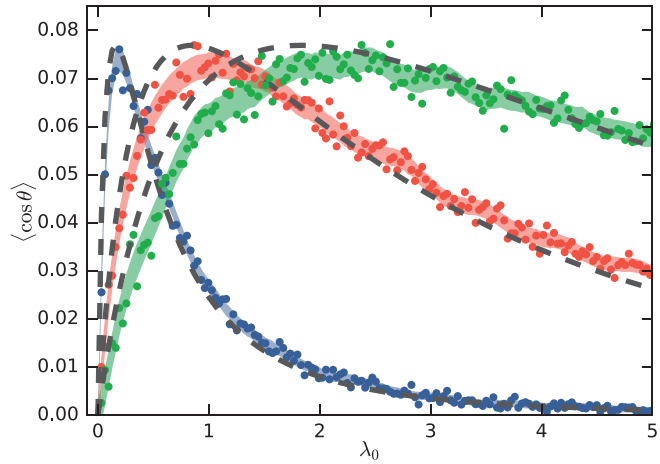

FIG. 4. Drift efficiency as a function of tumble frequency. Data from direct simulation of full model are shown for $k = 0$ (blue), $k = 3$ (red) and $k = 6$ (green). Each data point is the result of 10,000 simulations and shaded background indicates standard error with $D_r = 0.1\,\mathrm{s}^{-1}$, $\beta = 1/2$, $\gamma = 1\,\mathrm{s}^{-1}$. Linearized theory is indicated by dashed lines.

shown that an optimum base tumbling frequency λ_0 exists (Celani & Vergassola, 2010). Intuitively, in the low-noise limit, this optimum should be set by the rotational diffusion constant D_r in order to dominate rotational diffusion but not hinder drift. Intuitively, one expects that introducing persistence, which results in smaller angular deflections from tumbles, would shift the optimal tumble frequency to higher values. So while it is clear that persistence can increase the chemotactic drift for a given base tumble frequency, it is not clear what the effect is if variations in λ_0 are also allowed.

To study this, we simulated cells performing chemotaxis in a constant gradient for various persistence parameters k while varying λ_0. The results shown in Fig. 4 confirm the intuition outlined above; for large base tumbling frequency λ_0, increasing the persistence k leads to increased chemotactic drift, as previously found. However, for low values of λ_0 the opposite effect is found. There is thus a trade-off between frequency and persistence of tumbles.

To gain further insight we study the relevant Fokker–Planck equation. As shown previously (Celani & Vergassola, 2010), the dynamics of the biaser q can be made Markovian by introducing three internal variables (moments of c)

$$m_j = \int_{-\infty}^{t} e^{-\gamma(t-t')}(t-t')^j c(t')\,\mathrm{d}t', \tag{4.1}$$

which obey a coupled system of differential equations

$$\partial_t m_j = c(t)\delta_{j0} - \gamma m_j + j m_{j-1}. \tag{4.2}$$

It follows that the distribution function $P(x, \theta, \{m_j\}, t)$, describing the probability density that a cell at time t is at position x, swimming in direction θ and has internal variables with values $\{m_j\}$, obeys the

Fokker–Planck equation

$$\frac{\partial P}{\partial t} + v\cos\theta\,\frac{\partial P}{\partial x} = D_r\frac{\partial^2 P}{\partial \theta^2} + \lambda_0\lfloor 1+q(t)\rfloor\left[\int \frac{e^{k\cos(\theta-\theta')}}{2\pi I_0(k)}P(\theta')\,\mathrm{d}\theta' - P\right] - \sum_j \partial_{m_j}\left[\delta_{j,0}\,c(x) + jm_{j-1} - \gamma m_j\right]P, \tag{4.3}$$

where

$$q(t) = \frac{\beta\gamma^2}{\alpha\, v}\left(\frac{1}{2}\gamma^2 m_2 - \gamma m_1\right). \tag{4.4}$$

The left-hand side of (4.3) is the advective derivative with $v\cos\theta$ being the instantaneous velocity in the x-direction. On the right-hand side, the first term describes rotational diffusion. The second term describes tumbling with frequency $\lambda_0\lfloor 1+q(t)\rfloor$. The first term in the square bracket describes the probability mass gained by tumbles resulting in final angle θ and the second term describes probability mass lost by tumbles that start with angle θ. Finally, the last term of (4.3) implements the dynamics of the internal variables defined in (4.2).

We begin by solving this system analytically for small β. Later we will argue that our conclusions remain qualitatively correct also for large β. In steady state, we find (Appendix A)

$$\langle\cos\theta\rangle = \frac{\beta\gamma^3\lambda_k}{2(D_r+\lambda_k)(D_r+\gamma+\lambda_k)^3} + \mathcal{O}(\beta^2), \tag{4.5}$$

where $\lambda_k = \lambda_0\,[1 - I_1(k)/I_0(k)]$. Note that the only place λ_0 enters is through the quantity λ_k, which has the optimal value

$$\lambda_k^* = \frac{1}{3}\left(\sqrt{4D_r^2 + 3\gamma D_r} - D_r\right). \tag{4.6}$$

From this fact, we conclude that the trade-off between tumbling frequency and tumble persistence is perfectly balanced; changes in k can be precisely compensated by changes in λ_0.

Figure 4 shows how this small-β result accurately matches the full numerical results even for $\beta = 1/2$. So while persistence can lead to enhanced chemotaxis, we find that this has nothing inherently to do with the persistence of the tumbles themselves, as the same increase can be achieved simply by lowering the base tumbling frequency.

With constant λ_0, letting $k \to \infty$ results in negligible drift. For large k, $[1 - I_1(k)/I_0(k)]^{-1} \sim 2k$. Thus, we see that a continuous version of run and tumble (Kirkegaard *et al.*, 2016a) emerges in the limit $k \to \infty$ if λ_0 is scaled linearly with k, and we conclude that such a strategy is equally optimal to any other persistence of tumbles with the correct choice of tumble frequency. These results arise because we allow λ_0 to be chosen independently of γ. Without persistence, chemotaxis is optimized for λ_0 and γ of similar order. For cells with large persistence, however, optimization leads to λ_0 much larger than γ.

The above conclusions of perfect trade-off between λ_0 and k are made for $\langle\cos\theta\rangle$ using equations where second-order moments are neglected. By considering higher-order closures and by comparing to numerical simulations, we have found that the expansion $P(x,\theta,\{m_j\}) = a_0(x,\{m_j\}) + a_1(x,\{m_j\})\cos\theta$ captures the full steady-state distribution well, without the need for higher-order Fourier terms. The form of λ_k can only change if higher-order Fourier modes become important. This is not the case

even in the high-β regime, and so these conclusions are also valid there. Second-order effects such as small dependencies of the optimal γ on λ_0 and k could also perturb the result of perfect trade-off between tumble frequency and persistence. Furthermore, although we only considered the steady state here, the conclusions apply to the transient behaviour of the system. Our conclusions also hold in three dimensions as demonstrated in Appendix D.

Real bacteria are observed to have an angular distribution of tumbles with a non-zero mode (Berg & Brown, 1972). To model this, we consider the reorientation distribution $g(\theta,\theta') = \sum_{\pm} e^{k\cos(\pm\mu+\theta-\theta')}/4\pi I_0(k)$. This results in the substitution $I_1(k)/I_0(k) \to I_1(k)/I_0(k)\cos\mu$ in (4.5) (see Appendix B), leaving our conclusions unchanged. If the turns are biased in one direction (e.g. turning more clockwise than counterclockwise), such that $g(\theta,\theta') = e^{k\cos(\mu+\theta-\theta')}/2\pi I_0(k)$, the efficiency can surpass that of unbiased cells. In this case the optimum strategy involves cells that continuously rotate, modulating their rotation speed as they swim (Appendix C). While this is an interesting behaviour, such a bias is a 2D phenomenon, although a related optimality may exist in 3D.

The fact that no single persistence value is globally preferable fits well with the experimental variations seen between biological species. The question still remains, however, if there are other effects that could induce a preferred tumble persistence. So far we have assumed the tumbles to be instantaneous. Including a finite tumble time can change the conclusions. In particular, since the optimal tumbling frequency for persistent tumbles is large, adding a constant time for each tumble results in large amounts of time in which no chemotactic progress is made, hence disfavouring persistence, On the other hand, one would expect a persistent tumble to take less time than a full tumble. The average tumble time $\langle\tau\rangle$ should depend on the average angle turned. The precise form of this dependence will change with reorientation method. If the tumbling rotation is ballistic, the mean reorientation time should be proportional to the mean angle turned. If, on the other hand, the cell relies on a diffusive method (which includes simply not swimming), the reorientation time will be proportional to the mean of the squared angle. We parametrize this with the exponent ζ, with $\zeta = 1$ for ballistic reorientations and $\zeta = 2$ for diffusive and a mixture for values in-between. The mean tumbling time is thus

$$\langle\tau\rangle = \frac{\tau_0}{\pi I_0(k)}\int_0^\pi \delta^\zeta e^{k\cos\delta}\,\mathrm{d}\delta. \tag{4.7}$$

The insets of Fig. 5 show trajectories for ballistic diffusive and intermediate exponents. For small chemotactic strength it is easy to incorporate this effect. The fraction of time spent swimming will be $1/(1+\langle\tau\rangle\lambda_0)$, so we find

$$\langle\cos\theta\rangle \to \frac{1}{1+\langle\tau\rangle\lambda_0}\frac{\beta\gamma^3\lambda_k}{2(D_r+\lambda_k)(D_r+\gamma+\lambda_k)^3}. \tag{4.8}$$

Crucially, λ_0 now appears alone, and we thus expect a global optimum to appear. Figure 5 shows $\langle\cos\theta\rangle$ evaluated for various exponents. For ballistic ($\zeta = 1$) we find that full tumbles ($k = 0$) are optimal. For diffusive $\zeta = 2$, the continuous dynamics ($k \to \infty$) becomes optimal. In between, as shown in Fig. 5(b), a finite k optimum appears. A finite non-zero persistence also appears for diffusive scaling with an added constant, i.e. for (4.7) plus a constant.

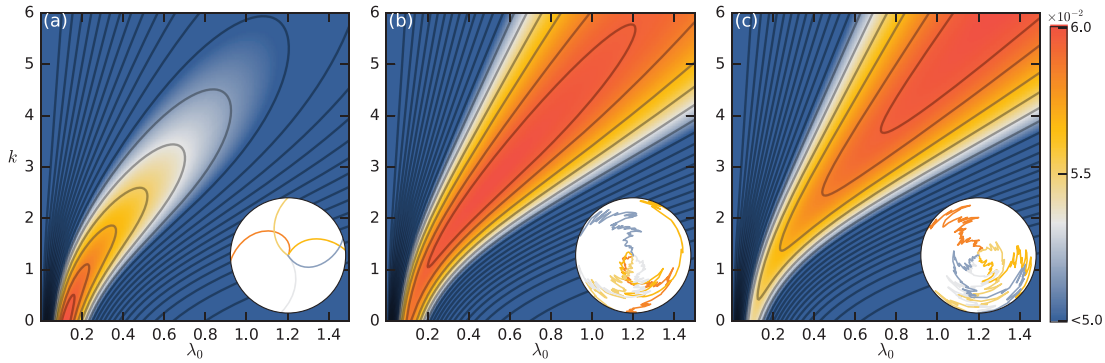

FIG. 5. Drift efficiency $\langle \cos\theta \rangle$ with finite tumbling time. Panels correspond to different tumble time exponents: (a) $\zeta = 1.0$, (b) 1.7 and (c) 2.0. Colour scale shows the top 20% range of drift velocities. Insets show examples of reorientation trajectories for with exponent ζ, the angle on the circle indicating the orientation and the radial distance indicating time. Common parameters: $D_r = 0.1\,\mathrm{s}^{-1}$, $\beta = 1/2$, $\gamma = 1\,\mathrm{s}^{-1}$, $\tau_0 = 1\,\mathrm{s}$.

5. Chemotactic strength

We now ask whether optimality exists for the chemotactic strength parameter β. Of course, in models linearized in β no such optimality can appear, and we must seek a different approach. Averaging over many numerical realizations of the model would allow these effects to be captured, but a large number of realizations is needed to gain accurate statistics, rendering parameter space exploration hard. Hence, we begin this section by gaining intuition through a more tractable model, which gives a good qualitative understanding of the problem.

The crucial insight for this simplified model is that in a constant gradient there is nothing to distinguish one value of the position variable x from another. In our full model, the biaser $q(t)$ relaxes to $-\beta$ times the cell's estimate of $\cos\theta$ on a timescale $\sim \gamma$. Such a behaviour can be modelled by the Langevin equation

$$\mathrm{d}q = -\frac{\gamma}{4}\,(q + \beta\cos\theta)\,\mathrm{d}t + \beta\sqrt{2\sigma}\,\mathrm{d}W, \tag{5.1}$$

where we now consider q as an effective representation of the internal parameters, instead of modelling the dynamics of internal parameters directly (and they, in turn, defining q). The prefactor of 1/4 is chosen so that the effective relaxation time matches that of the kernel κ used in the full model, and we have introduced a noise term (such a noise term plays no role in the linearized system). We can specify this system fully through a Fokker–Planck equation for $P(\theta, q, t)$,

$$\frac{\partial P}{\partial t} = \frac{\gamma}{4}\frac{\partial}{\partial q}(q + \beta\cos\theta)\,P + \sigma\beta^2\,\frac{\partial^2 P}{\partial q^2} + D_r\frac{\partial^2 P}{\partial \theta^2} + \lambda_0\lfloor 1 + q\rfloor\left[\int \frac{e^{k\cos(\theta-\theta')}}{2\pi I_0(k)}P(\theta')\,\mathrm{d}\theta' - P\right]. \tag{5.2}$$

Again we consider the steady-state behaviour. The optimal behaviour of the original system is well captured by this reduced model (Appendix E). Crucially, (5.2) is simple enough to be solved numerically using a hybrid spectral-finite difference method. We discretize q into $\{q_i\}$ and expand $P(\theta, q_i) = \sum_n a_{ni}\cos n\theta$. The differential q-operators in (5.2) are approximated by fourth-order central-difference schemes, and by orthogonality of $\cos\theta$ and the linearity of (5.2) we can numerically solve directly for the coefficients a_{ni}. We find that for all parameters the same efficiency ($\langle\cos\theta\rangle$) can be obtained for

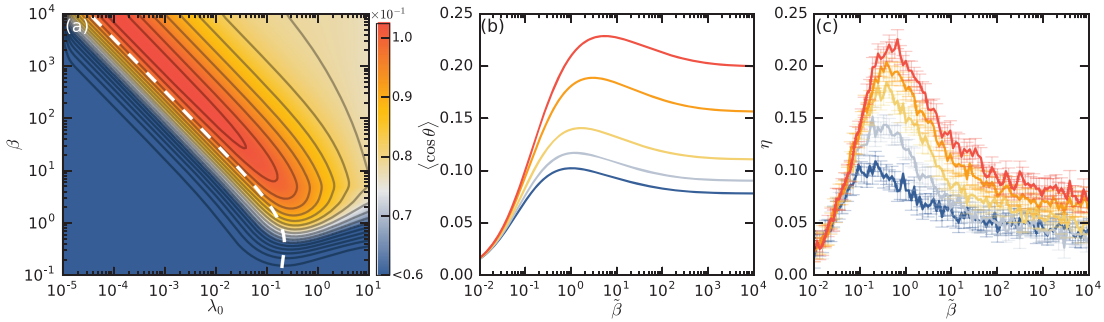

FIG. 6. Drift efficiency as a function of chemotactic strength. (a) Variations in β and λ_0 reveal a maximum as $\beta \to \infty$, $\lambda_0 \to 0$. Dashed curve is analytical approximation to optimum region. (b) Chemotactic drift with modulation of the form $\tilde{\beta}\lfloor q \rfloor$. Curves vary from $\sigma = 0.15$ (red) to $\sigma = 1.0$ (blue). (c) Full particle simulations with average molecules sensed by cells varying from 0.5 (blue) to 3 (red). Common parameters: $D_r = 0.1\,\mathrm{s}^{-1}$, $\beta = 1/2$, $\gamma = 1\,\mathrm{s}^{-1}$.

any k by a simple rescaling of λ_0. We thus set $k = 0$ in the remainder of this section without loss of generality.

Figure 6(a) shows the resulting chemotactic drift under variation of the chemotaxis strength β and the base tumbling frequency λ_0. For a given λ_0, an optimal chemotactic strength does indeed exist. Choosing the chemotactic strength too high, evidently, also results in too many tumbles. Figure 6(a) also shows, however, that under variations of both β and λ_0 the optimal is found for $\beta \to \infty$. For large β the optimum lies on a straight line (power law) relating β to λ_0.

To understand what sets the optimal chemotactic strength, we seek an analytical approach, but since there is no perturbative small parameter we examine instead a Fourier–Hermite expansion of the form

$$p(\theta, q) = \sum_{n=0}^{N} \sum_{m=0}^{M} a_{nm} \cos(n\theta)\, H_m(q/\zeta)\, e^{-q^2/\zeta^2}, \tag{5.3}$$

where H_m are the Hermite polynomials. The choice of this expansion arises from the fact that q resembles an Ornstein–Uhlenbeck process, the solution of which is Gaussian, with a scale ζ, which, for a true Ornstein–Uhlenbeck process would be $\sim \sqrt{4\sigma/\gamma}$. Presently, $\cos\theta$ also contributes to variations in q, and so $\zeta \sim \sqrt{1 + 4\sigma/\gamma}$. Here, we truncate at $N = M = 1$, which while yielding numerically inaccurate results nevertheless reveals the key dynamics. Higher-order terms can easily be calculated, but the expressions become lengthy. Exploiting orthogonality, the steady-state coefficients $\{a_{nm}\} = (a_{00}, a_{10}, a_{01}, a_{11})$ are found as the null space of

$$\begin{pmatrix} 0 & 0 & 0 & 0 \\ 0 & -\frac{\gamma}{4} & -\frac{\gamma}{8\zeta} & 0 \\ 0 & 0 & \frac{\lambda_0}{2}\mathrm{erfc}\left(\frac{1}{\zeta\beta}\right) - \frac{\lambda_0\zeta\beta}{2\sqrt{\pi}}\exp\left(\frac{-1}{\zeta^2\beta^2}\right) - \lambda_0 - D_r & -\frac{1}{2}\lambda_0\zeta\beta\left(1 + \mathrm{erc}\left(\frac{1}{\zeta\beta}\right)\right) \\ \frac{-\gamma}{4\beta} & 0 & -\frac{1}{4}\lambda_0\zeta\beta\left(1 + \mathrm{erf}\left(\frac{1}{\zeta\beta}\right)\right) & \frac{1}{2}\lambda_0\,\mathrm{erfc}\left(\frac{1}{\zeta\beta}\right) - \lambda_0\left(1 + \frac{\zeta\beta}{\sqrt{\pi}}\exp\left(\frac{-1}{\zeta^2\beta^2}\right)\right) \end{pmatrix}, \tag{5.4}$$

whence $\langle \cos\theta \rangle = a_{10}/(2\,a_{00})$. Optimizing this for λ_0 we obtain the dashed white curve in Fig. 6(a). In the limit $\beta \to \infty$ this has the form

$$\lambda_0 \sim \sqrt{\frac{D_r(D_r + \gamma/4)}{1 + 4\sigma/\gamma}}\,\frac{1}{\beta}. \tag{5.5}$$

Although the expansion does not quite capture the location of the optimum, the correct scaling is obtained. The global optimum is found at $\beta \to \infty$ and we learn that $\lambda_0\beta$ tends to a finite value in that limit. In detail, the optimization tries to diminish the base tumbling contribution in the expression $\lambda_0\lfloor 1+q\rfloor$ and the optimum is found in limit where $\lambda_0\lfloor 1+q\rfloor \to \lambda_0\lfloor q\rfloor$. Explicitly making this substitution in (5.2) and defining $\tilde{\beta} = \lambda_0\beta$, we obtain a system that has a finite optimal value of chemotactic strength. This is shown in Fig. 6 for various noise strengths σ. To verify our conclusions based on this model we turn to the full simulation. Exactly as in the simplified model, we find optimum behaviour after making the substitution $\lambda_0\lfloor 1+q\rfloor \to \lambda_0\lfloor q\rfloor$. This is shown in Fig. 6(c) for various levels of chemoattractant concentrations, confirming our conclusions.

It is perhaps surprising that the optimum is found in this limit, since no modulation of tumbling frequency then can occur if $q < 0$, which is the case when the cell swims just slightly in the correct direction, and thus in the limit of no noise, the angular distribution will be governed simply by rotational diffusion on $\theta \in [-\pi/2, \pi/2]$. In this optimal limit, the cells have minimized the time they spend swimming in any wrong direction, which, evidently, even though it leads to no active modulation for $q < 0$, is also the optimum for the total chemotactic drift. For stochastic taxis to work, the modulation must necessarily be a monotonically increasing function of q. Strong reaction when swimming in the wrong direction ($q > 0$) is thus typically coupled will smaller reaction when swimming in the correct direction ($q < 0$). Our results show, at least for the presently chosen form of modulation, that with this trade-off the best choice is to react very strongly when swimming in the wrong direction, even though this reduces the effectiveness of chemotaxis while swimming in the right direction.

6. Conclusions

In this study we have taken an approach to understanding run-and-tumble chemotaxis based on simultaneous parameter optimization. For the specific system studied here, cells in constant gradients, we have focused on the base tumbling frequency λ_0, tumbling persistence k and chemotactic strength β as key parameters. Varying any one parameter alone, there is a unique value that optimizes the chemotactic drift, but when all parameters are free there is a higher-dimensional optimal locus.

In particular, the trade-off in optimality between the base tumbling frequency and tumble persistence is 'perfect' in the sense that any increase, say, in persistence can be countered by an increase in base tumble frequency. After a persistent tumble, it would seem that the current value of q would stay more relevant than for a full tumble indicating that persistence could lead to enhanced chemotaxis. The intuition behind this argument is based on comparing a 'single' full tumble to a 'single' persistent tumble, but a more appropriate comparison would be to a 'series' of persistent tumbles. And as evident by our calculations, comparing in this way the argument of preservation of information leads to similar behaviour for all persistence parameters. One might also argue for the opposite: after a full tumble (or a series of persistent tumbles) there is a high risk that the new direction is wrong. Therefore, one could argue that keeping q large is a desirable strategy, since it increases the probability of correcting the tumble quickly. Our results show that both of these arguments are incorrect. Although one could

imagine a model in which q is explicitly altered after each tumble, say $q \to a\,q$, the study of this variant would require relaxing the assumption of fixed γ in order to find global optima.

Introducing a finite tumble time moves the model away from the perfect trade-offs described above. We have shown that an optimum persistence emerges that depends on the manner in which the tumble time depends on reorientation angle. For ballistic tumbles, zero persistence is optimal, while continuous tumbling is optimal for diffusive tumbles. A finite persistence emerges for exponents in-between, i.e. for tumbles that are superdiffusive but not ballistic. Such a tumble could simply be a mixture of ballistic and diffusive reorientations that when taken together have a superdiffusive behaviour. Diffusive tumbles are easy to generate: a cell can do so by simply not swimming and more generally by wiggling its flagella in random directions. Ballistic tumbles require directed motion of the flagella (even though the actual direction is chosen randomly). Actual tumbles might be a combination of a fixed tumble time plus a diffusive scaling, which would favour a finite tumble persistence (non-zero and non-infinite). One could furthermore imagine minimizing tumble times by maintaining a finite swimming speed during tumbles, e.g. via polymorphic transformations of the flagella (Goldstein *et al.*, 2000).

In addition to studying the weak chemotaxis limit, we have also investigated the effects of strong chemotaxis. While this is, naturally, dependent on the precise functional form chosen for the biasing of tumbles, we have shown that optima in chemotactic strength can also emerge. Through an analytical approximation we found that the form $\lambda_0\lfloor 1+q\rfloor$ has an optimal value of β for constant λ_0. Allowing for variations in λ_0 the optimum shifts to $\beta \to \infty$, and instead $\tilde{\beta} = \beta\lambda_0$ as $\beta \to \infty$ has an optimal value. This naturally leads to the question of the optimal form of the modulation. Preliminary results have shown that other simple choices, e.g. $\lambda_0\, e^q$, do not perform better than the form studied here. In general such problems can be considered partially observable Markov decision processes, and a potential optimal functional form could be found by methods such as reinforcement learning. Results from such analysis, however, will probably be strongly dependent on the model set-up, and a form that optimizes for drift in constant gradients will not necessarily do well in other gradients.

Comparing to experimental systems, our result that persistence does not have a unique optimum when allowing for variations in base tumble frequency fits well with the variation that exists between species. The chemotactic strength result that the optimum is found as $\lambda_0 \to 0$ is a special outcome of maximizing the drift velocity in a constant gradient. In more complex domains, the cells will need to react also to spatial variations (Appendix E) and thus need a finite λ_0 and smaller β. Maximizing the minimum chemotactic efficiency over many chemoattractant profiles reveals the experimental values associated with the kernel κ and base tumbling frequency (Celani & Vergassola, 2010). A linear approach cannot, however, reveal an optimal chemotactic strength. An interesting question for future research is thus: can maximizing the minimum chemotactic efficiency over suitably chosen noise models reveal an optimal finite chemotactic strength? While difficult to tackle analytically, numerical methods may be able to answer such questions.

Acknowledgements

It is a pleasure to dedicate this work to the memory of John Blake, whose impact on the mathematics of microorganism locomotion was so profound.

Funding

Engineering and Physical Sciences Research Council; St. John's College, Cambridge (to J.B.K.); Established Career Fellowship from the Engineering and Physical Science Research Council (to R.E.G.).

References

Berg, H. C. & Brown, D. A. (1972) Chemotaxis in Escherichia coli analysed by three-dimensional tracking. *Nature,* **239**, 500–504.

Berg, H. C. & Purcell, E. M. (1977) Physics of chemoreception. *Biophys. J.*, **20**, 193–219.

Bonner, J. T. & Savage, L. (1947) Evidence for the formation of cell aggregates by chemotaxis in the development of the slime mold Dictyostelium discoideum. *J. Exp. Zool.*, **106**, 1–26.

Celani, A. & Vergassola, M. (2010) Bacterial strategies for chemotaxis response. *Proc. Natl. Acad. Sci.*, **107**, 1391–1396.

Drescher, K., Goldstein, R. E. & Tuval, I. (2010) Fidelity of adaptive phototaxis. *Proc. Natl. Acad. Sci. USA*, **107**, 11171–11176.

Friedrich, B. M. & Julicher, F. (2007) Chemotaxis of sperm cells. *Proc. Natl. Acad. Sci. USA*, **104**, 13256–61.

Goldstein, R. E., Goriely, A., Huber, G. & Wolgemuth, C. W. (2000) Bistable helices. *Phys. Rev. Lett.*, **84**, 1631–1634.

Hein, A. M., Brumley, D. R., Carrara, F., Stocker, R. & Levin, S. A. (2016) Physical limits on bacterial navigation in dynamic environments. *J. Royal Soc.*, **13**, 20150844.

Jikeli, J. F., Alvarez, L., Friedrich, B. M. Wilson, L. G., Pascal, R., Colin, R., Pichlo, M., Rennhack, A., Brenker, C. & Kaupp, U. B. (2015) Sperm navigation along helical paths in 3D chemoattractant landscapes. *Nat. Comm.*, **6**, 7985.

Kirkegaard, J. B., Bouillant, A., Marron, A. O., Leptos, K. C. & Goldstein, R. E. (2016a) Aerotaxis in the closest relatives of animals. *eLife*, **5**, e18109.

Kirkegaard, J. B., Marron, A. O. & Goldstein, R. E. (2016b) Motility of colonial choanoflagellates and the statistics of aggregate random walkers. *Phys. Rev. Lett.*, **116**, 038102.

Locsei, J. T. (2007) Persistence of direction increases the drift velocity of run and tumble chemotaxis. *J. Math. Biol.*, **55**, 41–60.

Locsei, J. T. & Pedley, T. J. (2009) Run and tumble chemotaxis in a shear flow: the effect of temporal comparisons, persistence, rotational diffusion & cell shape. *Bull. Math. Biol.*, **71**, 1089–1116.

Mora, T. & Wingreen, N. S. (2010) Limits of sensing temporal concentration changes by single cells. *Phys. Rev. Lett.*, **104**, 248101.

Mortimer, D., Dayan, P., Burrage, K. & Goodhill, G. J. (2011) Bayes-optimal chemotaxis. *Neural Comput.*, **23**, 336–373.

Nicolau, D. V., Armitage, J. P. & Maini, P. K. (2009) Directional persistence and the optimality of run-and-tumble chemotaxis. *Comput. Biol. Chem.*, **33**, 269–274.

Peaudecerf, F. J. & Goldstein, R. E. (2015) Feeding ducks, bacterial chemotaxis & the Gini index. *Phys. Rev. E*, **92**. 022701.

Polin, M., Tuval, I., Drescher, K., Gollub, J. P. & Goldstein, R. E. (2009) Chlamydomonas swims with two 'gears' in a eukaryotic version of run-and-tumble locomotion. *Science*, **325**, 487–490.

Reneaux, M. & Gopalakrishnan, M. (2010) Theoretical results for chemotactic response and drift of E. coli in a weak attractant gradient. *J. Theor. Biol.*, **266**, 99–106.

Rivero, M. A., Tranquillo, R. T., Buettner, H. M. & Lauffenburger, D. A. (1989) Transport models for chemotactic cell populations based on individual cell behavior. *Chem. Eng. Sci.*, **44**, 2881–2897.

Segall, J. E., Block, S. M. & Berg, H. C. (1986) Temporal comparisons in bacterial chemotaxis. *Proc. Natl. Acad. Sci. USA*, **83**, 8987–8991.

Tindall, M. J., Maini, P. K., Porter, S. L. & Armitage, J. P. (2008a) Overview of mathematical approaches used to model bacterial chemotaxis II: bacterial populations. *Bull. Math. Biol.*, **70**, 1570–1607.

Tindall, M. J., Porter, S. L., Maini, P. K., Gaglia, G. & Armitage, J. P. (2008b) Overview of mathematical approaches used to model bacterial chemotaxis I: the single cell. *Bull. Math. Biol.*, **70**, 1525–1569.

Yoshimura, K. & Kamiya, R. (2001) The sensitivity of chlamydomonas photoreceptor is optimized for the frequency of cell body rotation. *Plant Cell Physiol.*, **42**, 665–672.

Appendix A. Linearized drift

To find the drift $\langle \cos\theta \rangle$ linearized in β, we multiply

$$\frac{\partial P}{\partial t} + v\cos\theta\,\frac{\partial P}{\partial x} = D_r \frac{\partial^2 P}{\partial \theta^2} + \lambda_0 \lfloor 1 + q(t) \rfloor \left[\int \frac{e^{k\cos(\theta-\theta')}}{2\pi I_0(k)} P(\theta')\,\mathrm{d}\theta' - P \right] - \sum_j \partial_{m_j}\left[\delta_{j,0}\, c(x) + j m_{j-1} - \gamma m_j\right] P, \tag{A.1}$$

by $\cos\theta$, whereafter integration yields

$$\partial_t \langle \cos\theta \rangle = -D_r \langle \cos\theta \rangle - \lambda_0 \left(1 - \frac{I_1(k)}{I_0(k)}\right) \left(\langle \cos\theta \rangle + \langle q \cos\theta \rangle \right), \tag{A.2}$$

using

$$\int e^{k\cos(\theta-\theta')} \cos\theta\,\mathrm{d}\theta = 2\pi I_1(k) \cos\theta'. \tag{A.3}$$

The last terms disappear by partial integration of m_j.

Since $q(t) = \frac{\beta\gamma^2}{\alpha v}(\gamma^2 m_2/2 - \gamma m_1)$ we continue neglecting quadratic terms

$$\partial_t \langle m_0 \cos\theta \rangle = -(D_r + \lambda_k + \gamma)\langle m_0 \cos\theta \rangle + \alpha \langle x \cos\theta \rangle, \tag{A.4}$$

$$\partial_t \langle m_1 \cos\theta \rangle = -(D_r + \lambda_k + \gamma)\langle m_1 \cos\theta \rangle + \langle m_0 \cos\theta \rangle, \tag{A.5}$$

$$\partial_t \langle m_2 \cos\theta \rangle = -(D_r + \lambda_k + \gamma)\langle m_2 \cos\theta \rangle + 2\langle m_1 \cos\theta \rangle, \tag{A.6}$$

$$\partial_t \langle x \cos\theta \rangle = \frac{v}{2} - (D_r + \lambda_k)\langle x \cos\theta \rangle. \tag{A.7}$$

Solving these equations for the steady state, one finds the result of the main text.

Appendix B. Linearized with mean tumble angle

The reorientation distribution is now

$$g_k(\theta, \theta') = \frac{1}{4\pi I_0(k)} \left(e^{k\cos(\theta-\theta'-\mu)} + e^{k\cos(\theta-\theta'+\mu)} \right) \tag{B.1}$$

such that

$$\partial_t \langle \cos\theta \rangle = -D_r \langle \cos\theta \rangle - \lambda_0 \left(1 - \frac{I_1(k)}{I_0(k)} \cos\mu\right) \left(\langle \cos\theta \rangle + \langle q \cos\theta \rangle \right), \tag{B.2}$$

where we used that $\cos\mu$ is an even function and $\sin\mu$, an odd function. So having a finite μ corresponds to changing the persistence. At precisely $\mu = \pm\pi/2$, persistence no longer changes the behaviour.

Appendix C. Linearized with mean tumble angle—biased direction

Here we take

$$g_k(\theta,\theta') = \frac{1}{2\pi I_0(k)} e^{k\cos(\theta-\theta'-\mu)}. \tag{C.1}$$

We now have

$$\begin{aligned}\partial_t\langle\cos\theta\rangle =& -D_r\langle\cos\theta\rangle - \lambda_0\left(1-\frac{I_1(k)}{I_0(k)}\cos\mu\right)(\langle\cos\theta\rangle + \langle q\cos\theta\rangle)\\ &- \lambda_0\frac{I_1(k)}{I_0(k)}\sin\mu\,(\langle\sin\theta\rangle + \langle q\sin\theta\rangle)\,.\end{aligned} \tag{C.2}$$

And then

$$\begin{aligned}\partial_t\langle m_0\cos\theta\rangle =& -D_r\langle m_0\cos\theta\rangle - \lambda_0\left(1-\frac{I_1(k)}{I_0(k)}\cos\mu\right)\langle m_0\cos\theta\rangle\\ &- \lambda_0\frac{I_1(k)}{I_0(k)}\sin\mu\langle m_0\sin\theta\rangle + \alpha\langle x\cos\theta\rangle - \gamma\langle m_0\cos\theta\rangle,\end{aligned} \tag{C.3}$$

$$\begin{aligned}\partial_t\langle m_1\cos\theta\rangle =& -D_r\langle m_1\cos\theta\rangle - \lambda_0\left(1-\frac{I_1(k)}{I_0(k)}\cos\mu\right)\langle m_1\cos\theta\rangle\\ &- \lambda_0\frac{I_1(k)}{I_0(k)}\sin\mu\langle m_1\sin\theta\rangle + \langle m_0\cos\theta\rangle - \gamma\langle m_0\cos\theta\rangle,\end{aligned} \tag{C.4}$$

$$\begin{aligned}\partial_t\langle m_2\cos\theta\rangle =& -D_r\langle m_2\cos\theta\rangle - \lambda_0\left(1-\frac{I_1(k)}{I_0(k)}\cos\mu\right)\langle m_2\cos\theta\rangle\\ &- \lambda_0\frac{I_1(k)}{I_0(k)}\sin\mu\langle m_2\sin\theta\rangle + 2\langle m_1\cos\theta\rangle - \gamma\langle m_2\cos\theta\rangle,\end{aligned} \tag{C.5}$$

$$\begin{aligned}\partial_t\langle x\cos\theta\rangle =& \frac{v}{2} - D_r\langle x\cos\theta\rangle - \lambda_0\left(1-\frac{I_1(k)}{I_0(k)}\cos\mu\right)\langle x\cos\theta\rangle\\ &- \lambda_0\frac{I_1(k)}{I_0(k)}\sin\mu\langle x\sin\theta\rangle\end{aligned} \tag{C.6}$$

and similarly for the $\sin\theta$ terms, except no $v/2$ term appears in the equation for $\partial_t\langle x\sin\theta\rangle$.

This can be solved for the steady solution of $\langle \cos\theta \rangle$, but the expression is quite lengthy. Analysing it, we find that the optimum is found for $k \to \infty$. Taking this limit we find

$$\begin{aligned}\langle \cos\theta \rangle \to \beta\gamma^3\lambda_0 \Big[& \lambda_0^2(\cos(2\mu)(3(\gamma + D_r + \lambda_0)(\gamma + 2(D_r + \lambda_0)) + \lambda_0(3\gamma + 4(D_r + \lambda_0))) \\ & + \lambda_0(\cos(3\mu)(-3\gamma - 4D_r - 5\lambda_0) + \lambda_0 \cos(4\mu))) - \cos\mu(\gamma + D_r + \lambda_0)\big(\lambda_0^2(10\gamma + 17D_r) \\ & + \lambda_0(\gamma + D_r)(2\gamma + 7D_r) + D_r(\gamma + D_r)^2 + 11\lambda_0^3\big) + (\gamma + D_r + \lambda_0)^2((D_r + \lambda_0)(\gamma + D_r + \lambda_0) \\ & + \lambda_0(\gamma + 4(D_r + \lambda_0)))\Big] \Big/ \Big[2\big(- 2\lambda_0(D_r + \lambda_0)\cos\mu + (D_r + \lambda_0)^2 + \lambda_0^2\big) \\ & \big(-2\lambda_0 \cos\mu(\gamma + D_r + \lambda_0) + (\gamma + D_r + \lambda_0)^2 + \lambda_0^2\big)^3\Big]. \end{aligned} \tag{C.7}$$

The optimum is found at $\mu \to 0$, $\lambda_0 \to \infty$, keeping $\lambda_0\mu$ constant. The motion is thus continuously rotating cells, where the rotation speed is modulated by the chemoattractants.

Appendix D. Persistence in 3D

The linearized calculation is very similar in 3D. Defining p as a unit vector in the swimming direction, we can write the Fokker–Planck equation with von Mises tumbles as

$$\begin{aligned}\frac{\partial P(t,x,p,m)}{\partial t} + v\,p_x\,\frac{\partial P}{\partial x} = & D_r\nabla_p^2 P + \lambda_0\lfloor 1 + q(t)\rfloor\left[\int \frac{k\,e^{k\,p\cdot p'}}{4\pi\,\sinh k} P(p')\,\mathrm{d}\Omega' - P\right] \\ & - \sum_j \partial_{m_j}\big[\delta_{j,0}\,c(x) + jm_{j-1} - \gamma m_j\big]P,\end{aligned} \tag{D.1}$$

where ∇_p^2 is the angular Laplacian.

This leads to

$$\partial_t\langle p_x\rangle = -2D_r\langle p_x\rangle - \lambda_0\left[1 + \frac{1}{k} - \frac{1}{\tanh k}\right](\langle p_x\rangle + \langle q\,p_x\rangle), \tag{D.2}$$

showing an only slightly altered persistence modification to λ_k compared to 2D, and thus leading to similar conclusions as in 2D.

Appendix E. Simplified effective model

Figure E7 shows the performance of the simplified model of (5.2) compared to the simulations shown in Fig. 4.

Appendix F. Run and tumble in discrete 1D

In this section we study run and tumble in one spatial dimension. Such simplifications have proven to yield much insight in the case of no noise (Rivero *et al.*, 1989). For the present purpose we will

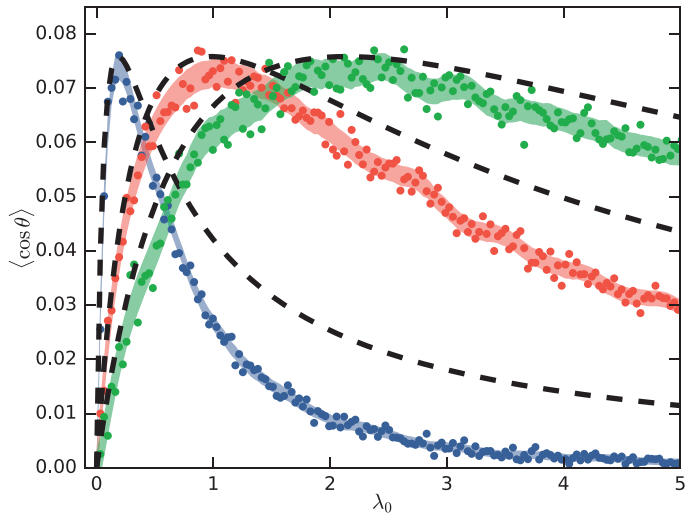

FIG. E7. Similar to Fig. 4 but with theoretical curves (dashed) obtained from the analysis of (5.2).

consider the case of a very noisy signal. To simplify further we put the cells and chemoattractants on an equilateral grid. We assume that each measurement carries the same error σ. In reality, the measurement of a concentration c has an error $\propto \sqrt{c}$, but such effects are expected to be second order. Thus, at each grid position i, the cell measures a concentration $c_i \sim \mathcal{N}(c(\boldsymbol{x}_i), \sigma^2)$, where $c(\boldsymbol{x}_i)$ is the time average of the signal at that position.

In particular, a cell will swim n lattice points and calculate $Q = \sum_j k_j c_{i(j)}$, where k_j is some kernel, reminiscent of the continuous kernel used in the main text. In the simplest model, if $Q > 0$ the cell will keep going in the same direction but turn if $Q < 0$. We begin by determining the optimal $\{k_j\}$.

F.1 *Optimal kernel*

We determine $\{k_j\}$ in such a way that Q makes the best estimate of a constant gradient. Thus, we consider $c_i = \mathcal{N}(c_0 + \alpha i), \sigma^2)$. Then $Q = \sum k_j c_j$ is an unbiased estimator of α if

$$\langle Q \rangle = \sum k_j \langle c_j \rangle = \sum k_j (c_0 + \alpha j) = c_0 \sum k_j + \alpha \sum k_j j = \alpha, \tag{F.1}$$

so we must require $\sum k_j = 0$ and $\sum k_j j = 1$. The variance becomes

$$\mathrm{Var} Q = \langle Q^2 \rangle - \langle Q \rangle^2 = \sigma^2 \sum k_j^2. \tag{F.2}$$

Writing $Q = \sum k_i c_i$, minimizing the variance subject to the unbiased estimation yields

$$k_i = \frac{6(2i - n_1 - n_2)}{(n_2 - n_1 + 2)(n_2 - n_1 + 1)(n_2 - n1)} \tag{F.3}$$

for a measurement on $[n_1, n_2]$. Thus,

$$k_j = \frac{6(2j-n)}{(n+2)(n+1)n}, \tag{F.4}$$

where $n = n_2 - n_1$. Assuming a Gaussian distribution we thus have

$$Q \sim \mathcal{N}\left(\alpha, \sigma^2 \sum k_j^2\right) = \mathcal{N}\left(\alpha, \frac{12\sigma^2}{(n+2)(n+1)n}\right) \equiv \mathcal{N}\left(\alpha, \sigma_n^2\right). \tag{F.5}$$

F.2 *Chemotaxis in a constant gradient*

The probability that $Q < 0$ after a swim of n lattice points follows a geometric distribution with parameter

$$q = \frac{1}{\sqrt{2\pi\sigma^2}} \int_{-\infty}^{0} e^{-(x-\alpha)^2/2\sigma_n^2} \, \mathrm{d}x = \frac{1}{2} \operatorname{erfc}\left(\frac{\alpha}{\sqrt{2\sigma_n^2}}\right). \tag{F.6}$$

After a run left and right, the cell will have travelled on average

$$\frac{n}{q} - \frac{n}{1-q}, \tag{F.7}$$

while in that time it could have travelled on average the distance

$$\frac{n}{q} + \frac{n}{1-q}. \tag{F.8}$$

The efficiency is thus $\eta = 1 - 2q$, which is maximized for $q \to 0$, corresponding to $n \to \infty$. This is in the absence of spatial variations and diffusion effects.

F.3 *Effective rotational diffusion*

We now add the feature that after each jump the particle will flip either because $Q < 0$ or another process $R < 0$, which has parameter D_r for a single jump. The probability $R < 0$ after n jumps will thus be $r = 1 - (1 - D_r)^n$. Thus, the probability of a turn after the n jumps is $\tilde{q} = q + r - qr$ when going right and when going left $\tilde{p} = (1 - q) + r - (1 - qr)$. Calculating the efficiency we thus find

$$\eta = \frac{(1-2q)\,(1-D_r)^n}{2 - (1-D_r)^n}, \tag{F.9}$$

where q is defined as in (F.6). This defines an optimal n as shown in Fig. F8. The emergence of an optimal n corresponds to the emergence of an optimum γ in the main text.

F.4 *Chemotaxis in a spatially varying gradient*

Spatial variation from linear concentration profiles can also affect the optimal choice of n. Consider cells swimming in a gradient being held to a fixed value $c_0 > 0$ at the origin. The diffusion equation allows

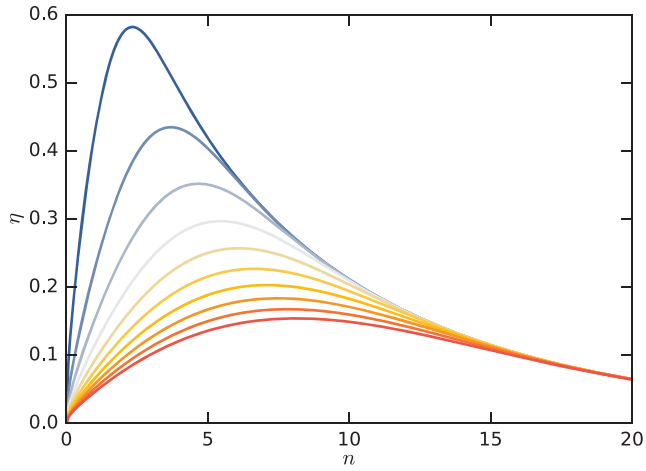

FIG. F8. Efficiency η as a function of n as in (F.9). Noise varies from $\sigma/\alpha = 1$ (blue) to $\sigma/\alpha = 10$ (red). $D_r = 0.1\,\mathrm{s}^{-1}$.

for linear steady-state solutions. We thus consider 1D swimmers in

$$c(x) = c_0 - \alpha|x|. \tag{F.10}$$

We again discretize space and allow the cells to choose an n, the number of lattice points to swim before making a decision on whether to change direction. This n determines σ_n and thus q. This also makes the cells only visit sites that are multiples of n and we thus reindex by that. We further note that a state moving right at position i is by symmetry the same as moving left at site $-i$. We exploit this symmetry and consider only $i \geqslant 0$. Our states are then called

$$(i,\, s) \in \mathbb{N}_0 \times \{+,-\} = \{(0,+),(0,-),(1,+),(1,-),(2,+),(2,-),\cdots\}. \tag{F.11}$$

The jumps form an infinite-dimensional Markov chain with transition matrix

$$\mathbb{T} = \begin{pmatrix}
0 & 0 & 0 & p & 0 & 0 & 0 & 0 & 0 & \cdots \\
0 & 0 & 0 & q & 0 & 0 & 0 & 0 & 0 & \cdots \\
p & q & 0 & 0 & 0 & p & 0 & 0 & 0 & \cdots \\
q & p & 0 & 0 & 0 & q & 0 & 0 & 0 & \cdots \\
0 & 0 & p & 0 & 0 & 0 & 0 & p & 0 & \cdots \\
0 & 0 & q & 0 & 0 & 0 & 0 & q & 0 & \cdots \\
0 & 0 & 0 & 0 & p & 0 & 0 & 0 & 0 & \cdots \\
0 & 0 & 0 & 0 & q & 0 & 0 & 0 & 0 & \cdots \\
0 & 0 & 0 & 0 & 0 & 0 & p & 0 & 0 & \cdots \\
0 & 0 & 0 & 0 & 0 & 0 & q & 0 & 0 & \cdots \\
\vdots & \vdots & \vdots & \vdots & \vdots & \vdots & \vdots & \vdots & \vdots & \ddots
\end{pmatrix}, \tag{F.12}$$

where $p = 1 - q$. The steady-state distribution is found by solving

$$\mathbf{p} = \mathbb{T}\,\mathbf{p}. \tag{F.13}$$

To solve this infinite set of equations, we truncate in an appropriate manner at m equations and then let $m \to \infty$. We assume m even and to conserve probability, for finite m set $\mathbb{T}_{m-1,m-1} = p$ and $\mathbb{T}_{m,m-1} = q$. This leads to

$$p_{i,s} = \frac{1}{A} \cdot \begin{cases} \frac{q^k}{p^{k-2}(1-2q+2q^2)} & (0,+) \\ \frac{q^{k+1}}{p^{k-1}(1-2q+2q^2)} & (0,-) \\ \frac{q^{k-i}}{p^{k-i}} & (i \geqslant 1,+) \\ \frac{q^k}{p^{k-2}(1-2q+2q^2)} & (1,-) \\ \frac{q^{k-i+1}}{p^{k-i+1}} & (i \geqslant 2,-) \end{cases} \tag{F.14}$$

where $k = m/2 - 2$ and A is a normalization constant determined by

$$\sum_{i,s} p_{i,s} = 1. \tag{F.15}$$

After a long calculation we find (for $q > 1/2$) in the limit $m \to \infty$,

$$\langle |x| \rangle = \frac{\Delta x\, n}{2} \left(2 - \frac{1}{q(n)} + \frac{1}{2q(n) - 1} \right). \tag{F.16}$$

Figure F9 shows a minimum appearing for large noise. Thus, we see that an optimal measurement distance must also be balanced with potential spatial variations not just with rotational diffusion.

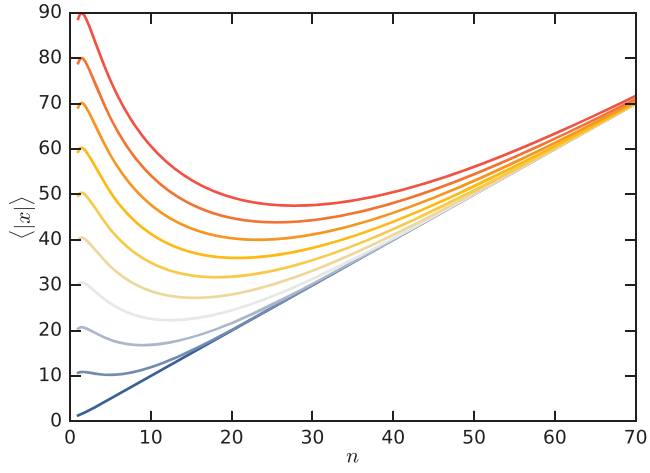

FIG. F9. Average position |x| for as a function of n, the number of jumps before deciding to change direction, as described by (F16). Chemotaxis is optimal when ⟨|x|⟩ is minimized, since the chemoattractant concentration decreases from $x = 0$. Parameters as in Fig. F8.